separations

MDPI

Article

Enantiomeric Separation and Molecular Modelling of Bioactive 4-Aryl-3,4-dihydropyrimidin-2(1*H*)-one Ester Derivatives on Teicoplanin-Based Chiral Stationary Phase

Isabella Bolognino [1,*,†], Antonio Carrieri [1], Rosa Purgatorio [1], Marco Catto [1], Rocco Caliandro [2], Benedetta Carrozzini [2], Benny Danilo Belviso [2], Maria Majellaro [3], Eddy Sotelo [3], Saverio Cellamare [1] and Cosimo Damiano Altomare [1,*]

[1] Department of Pharmacy-Pharmaceutical Sciences, University of Bari Aldo Moro, Via Orabona 4, 70125 Bari, Italy; antonio.carrieri@uniba.it (A.C.); rosa.purgatorio@uniba.it (R.P.); marco.catto@uniba.it (M.C.); saveriocellamare56@gmail.com (S.C.)

[2] Institute of Crystallography, CNR, Via Giovanni Amendola, 122/O, 70126 Bari, Italy; rocco.caliandro@ic.cnr.it (R.C.); benedetta.carrozzini@ic.cnr.it (B.C.); danilo.belviso@ic.cnr.it (B.D.B.)

[3] Singular Research Center in Biological Chemistry and Molecular Materials (CIQUS), University of Santiago de Compostela, 15782 Santiago de Compostela, Spain; ma.majellaro@usc.es (M.M.); e.sotelo@usc.es (E.S.)

* Correspondence: isabella.bolognino@unibg.it (I.B.); cosimodamiano.altomare@uniba.it (C.D.A.); Tel.: +39-080-5442781 (C.D.A.)

† Current address: Department of Engineering and Applied Sciences, University of Bergamo, Viale G. Marconi 5, 24044 Dalmine, Italy.

check for updates

Citation: Bolognino, I.; Carrieri, A.; Purgatorio, R.; Catto, M.; Caliandro, R.; Carrozzini, B.; Belviso, B.D.; Majellaro, M.; Sotelo, E.; Cellamare, S.; et al. Enantiomeric Separation and Molecular Modelling of Bioactive 4-Aryl-3,4-dihydropyrimidin-2(1*H*)-one Ester Derivatives on Teicoplanin-Based Chiral Stationary Phase. *Separations* **2022**, *9*, 7. https://doi.org/10.3390/separations9010007

Academic Editor: Jun Haginaka

Received: 23 November 2021
Accepted: 22 December 2021
Published: 28 December 2021

Publisher's Note: MDPI stays neutral with regard to jurisdictional claims in published maps and institutional affiliations.

Copyright: © 2021 by the authors. Licensee MDPI, Basel, Switzerland. This article is an open access article distributed under the terms and conditions of the Creative Commons Attribution (CC BY) license (https://creativecommons.org/licenses/by/4.0/).

Abstract: The enantiomeric separation of 15 racemic 4-aryl-3,4-dihydropyrimidin-2(1*H*)-one (DHP) alkoxycarbonyl esters, some of which proved to be highly active as A_{2B} adenosine receptor antagonists, was carried out by HPLC on Chirobiotic™ TAG, a chiral stationary phase (CSP) bearing teicoplanin aglycone (TAG) as the chiral selector. The racemic compounds were separated under polar organic (PO) conditions. Preliminarily, the same selectands were investigated on three different Pirkle-type CSPs in normal-phase (NP) conditions. A baseline separation was successfully obtained on TAG-based CSPs for the majority of compounds, some of which achieved high enantioselectivity ratios ($\alpha > 2$) in contrast with the smaller α values (1–1.5) and the lack of baseline resolution observed with the Pirkle-type CSPs. In particular, the racemic tetrazole-fused DHP ester derivatives, namely compounds **8** and **9**, were separated on TAG-based HPLC columns with noteworthy α values (8.8 and 6.0, respectively), demonstrating the potential of the method for preparative purposes. A competition experiment, carried out with a racemic analyte (**6**) by adding *N*-acetyl-D-alanine (NADA) to the mobile phase, suggested that H-bonding interactions involved in the recognition of the natural dipeptide ligand D-Ala-D-Ala into the TAG cleft should be critical for enantioselective recognition of 4-aryl DHPs by TAG. The X-ray crystal structure of TAG was elucidated at a 0.77 Å resolution, whereas the calculation of molecular descriptors of size, polar, and H-bond interactions, were complemented with molecular docking and molecular dynamics calculations, shedding light on repulsive (steric effects) and attractive (H-bond—polar and apolar) interactions between 4-aryl DHP selectands and TAG chiral selectors.

Keywords: 4-aryl-3,4-dihydropyrimidin-2(1*H*)-ones; teicoplanin aglycone; chiral HPLC; enantioselectivity; molecular docking; molecular dynamics

1. Introduction

The development and optimisation of methods to obtain enantiomers with high optical purity remain an important goal to be achieved in the early stages of drug discovery, considering that single enantiomers and diastereoisomers could often have distinct profiles in pharmacodynamics, pharmacokinetics, metabolism, and toxicity [1]. Within the variety of methods used, enantiomers' separation by high-performance liquid chromatography

(HPLC) has great impact in pharmaceutical research. A literature survey indicates that chiral stationary phases (CSPs) in enantioselective HPLC is the method of choice as it allows the overcoming of limitations such as, to name a few, the demand on the enantiomeric purity of the derivatizing agent when opting for off-line diastereomeric formation, chiral selector consumption, and detection interference when adding a chiral auxiliary to the mobile phase.

In this study, we report on the enantiomeric separation of a novel class of chiral bioactive 3,4-dihydropyrimidin-2(1*H*)-one (DHP) alkoxycarbonyl esters (Figure 1), mostly bearing an aryl group at C4, discovered by some of us as being potent and selective A_{2B} adenosine receptor (A_{2B}AR) antagonists. The investigated DHP derivatives were assembled in excellent yields by modification of the versatile and highly robust Biginelli reaction [2,3], a three-component transformation involving the catalysed condensation of a 1,3-dinucleophile (urea/thiourea or cyclic derivatives), and an aldehyde and β-ketoester [4]. A diverse series of DHP derivatives were explored [5–11] and optimal substituents in different positions of the heterocyclic core were identified as follows: (i) 2- or 3-furyl as well as 2- or 3-thienyl moiety at C4, (ii) ethyl or isopropyl ester group at C5, (iii) a methyl group at C6, and (iv) NH at position 1. Further diversification of the original 4-aryl-DHP scaffold [5,12–15] produced new ligands with improved affinity and selectivity profiles. Among others DHP derivatives, compounds **6**, **7**, **12**, and **13** were disclosed as highly potent A_{2B}AR selective antagonists [5,6,9], and the observed structure-activity relationships (SARs) were fully supported by molecular docking calculations.

Regarding the enantioselective binding of racemic DHPs to A_{2B}AR, it was demonstrated that the receptor affinity is almost exclusively due to the (*S*)-enantiomer [6,8–11]. The pharmacological evaluation of chiral DHP ligands investigated herein, **6**, **7**, and **13**, resolved into their enantiomers by chiral HPLC with polysaccharide-based CSPs in NP mode, demonstrated highly enantioselective recognition at the A_{2B}AR binding site, with the eutomers (*S*) showing K_i values in the low nanomolar range (6.30, 15.1, and 11.1 nM for **6**, **7**, and **13**, respectively) and the distomers (*R*) achieving less than 25% inhibition in all cases [6,11]. The enantioselective binding modes were investigated by molecular docking calculations, which suggested key H-bonding interactions between the DHP ligands and A_{2B}AR [6,11].

Fifteen representative racemic 4-aryl DHP derivatives (Figure 1), synthesised in the framework of the above-mentioned long-lasting research program, were selected from a large molecular library of the Sotelo group, considering the structural diversity and spread of pharmacological potency as selective A_{2B}AR antagonists. In previous studies, a good semi-preparative enantiomeric resolution of a number of racemic DHP derivatives was achieved using chiral HPLC with the polysaccharide-based (cellulose or amylose backbone) CSPs, whereas in this study we report on the investigation of teicoplanin-based CSPs, namely Chirobiotic™ TAG, which bears teicoplanin aglycone (TAG) as the chiral selector [16] in polar organic mode (POM) [17] as a suitable chiral HPLC method for the enantiomeric resolution of the racemic bioactive DHPs **1**–**15**.

TAG was preferred over the native glycosylated teicoplanin (TE) as chiral selector, based on the achievements of several studies [18]. Among racemic compounds resolved with teicoplanin-based stationary phases, for 5-methyl-5-phenylhydantoin and α-methyl-α-phenylsuccinimide the enantioselectivity factor (α) values determined on TAG-based CSPs were greater than those achieved with the native glycosylated TE chiral selector. Aryl sulfoxides proved particularly useful in studies aimed at understanding the multifactorial enantiorecognition mechanism on CSPs containing macrocyclic glycopeptide antibiotic as chiral selectors [19,20], and data showed a superior enantiodiscrimination capacity of TAG compared to TE under polar organic conditions [21].

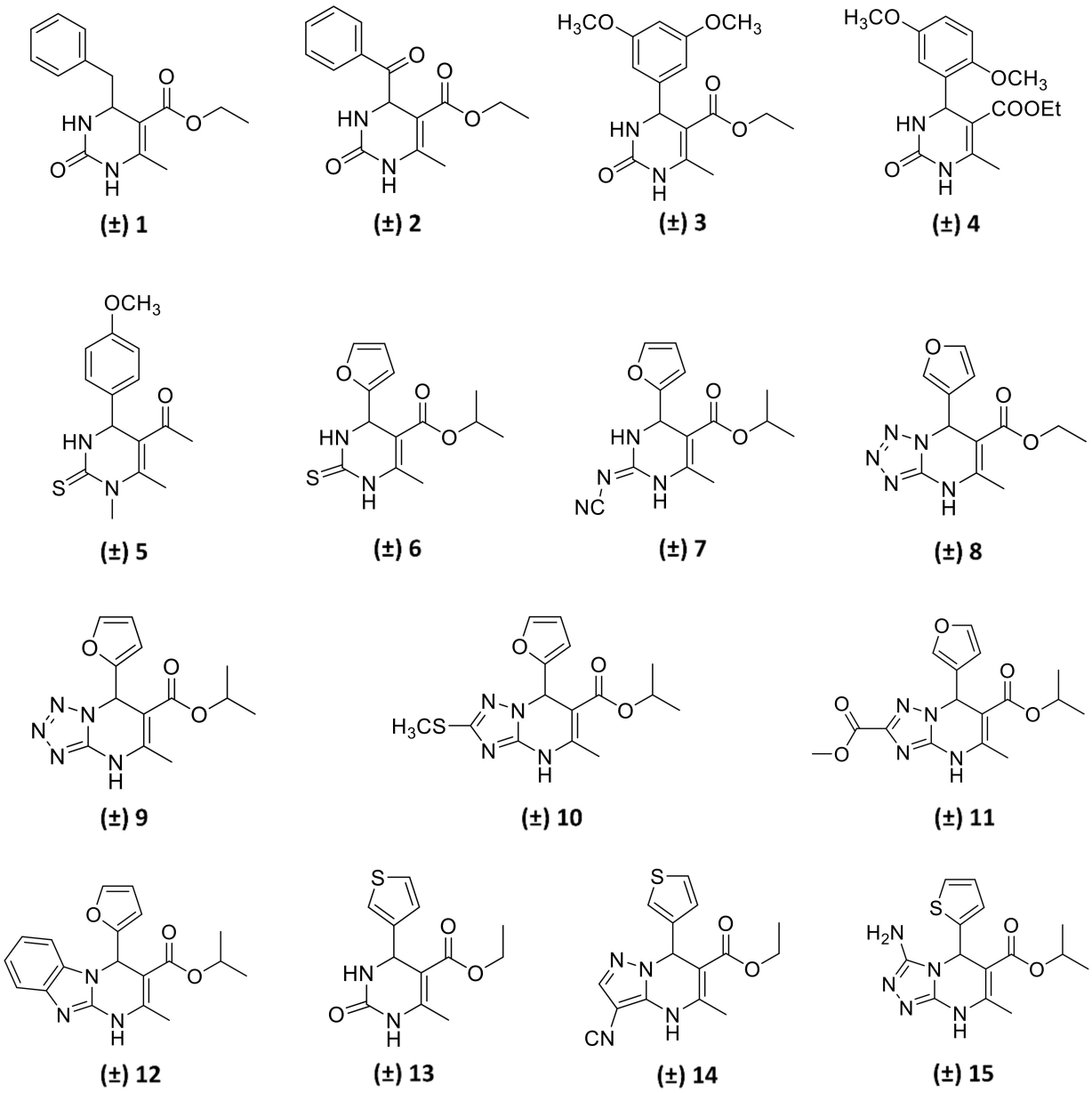

Figure 1. Structures of the examined chiral 4-aryl-substituted 3,4-dihydropyrimidin-2(1*H*)-one (DHP) ester derivatives. The biological activity of compounds **8**–**11** and **14**–**15** will be published elsewhere.

The enantioselective separations of the anticancer drug ifosfamide and its metabolites were successfully achieved on TAG under PO conditions, and a computational model suggested the network of HB interactions and cation-π interactions between the phosphoramide moiety and the aromatic components of the aglycon basket, which are fully consistent with the observed enantioselectivity [22].

Preliminary to the study of the chiral separation of DHP selectands on Chirobiotic™ TAG, three diverse Pirkle-type CSPs (Figure 2) were investigated in isocratic normal-phase (NP) conditions, with the aim of evaluating the effects on chiral recognition of π-π interactions, H-bonds, and repulsive steric factors. We use a computational protocol, similar to that previously adopted by us for another class of chiral selectands and diverse CSPs [23], to gain insights into the structure–enantioselective retention relationships and physicochemical interactions primarily responsible for the chiral recognition of the DHP selectands by TAG chiral selector, whose crystal structure has been solved herein by X-ray diffraction.

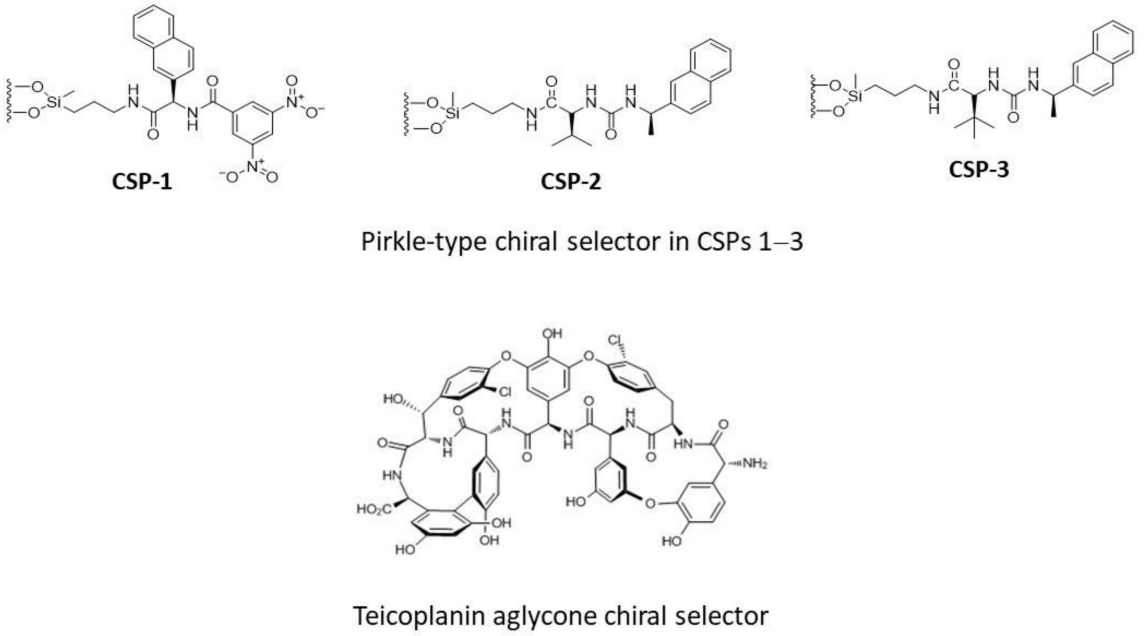

Figure 2. Chiral selectors of the CSPs investigated in this study.

2. Materials and Methods

2.1. Chemicals

All the analytical reagents and HPLC-grade solvents were purchased from Sigma-Aldrich (Milan, Italy). Ultrapure water was purified by a Milli-Q system.

Most of the racemic 4-substituted 3,4-dihydropyrimidin-2(1*H*)-one ester derivatives **1**–**15** were already synthesised by the Sotelo group in the Singular Research Center in Biological Chemistry and Molecular Materials (CIQUS), University of Santiago de Compostela (Spain), with Biginelli-based procedures using different 1,3-dinucleophiles, aldehydes, and β-ketoesters [5–11]. The UV spectra of racemic compounds **6**, **11** and **12**, taken as representative of the different chromophores examined in this study are shown in Figure S3 (Supplementary Materials).

Compounds **5**, **8**, **9**, **10**, **11**, **14**, and **15** were prepared according to the following general procedure. Analytical, physicochemical, and biological data of these compounds will be reported elsewhere.

Compounds **5**, **10**, and **11**: A mixture of the appropriate 1,3-dinucleophile (N-methyl thiourea, 3-(methylthio)-3*H*-1,2,4-triazol-5-amine or methyl 5-amino-3*H*-1,2,4-triazole-3-carboxylate; 1.5 eq), the corresponding aldehyde (4-methoxy benzaldehyde, 2-furaldehyde or 3-furaldehyde; 1 eq), the desired β-ketoester (pentane-2,4-dione, or isopropyl 3-oxobutanoate; 1 eq), and chloroacetic acid (0.1 eq) in THF (3 mL) was stirred at 90 °C for 12 h. The reaction was monitored by TLC and upon completion, the solvent was evaporated and the residue was purified by flash chromatography on silica gel (Hex:AcOEt).

Compounds **8** and **9**: A mixture of 1*H*-tetrazol-5-amine (1.5 eq), the corresponding aldehyde (2-furaldehyde or 3-furaldehyde; 1 eq), β-ketoester (ethyl 3-oxobutanoate or isopropyl 3-oxobutanoate; 1 eq), and L-proline (0.1 eq) in DMF (3 mL) was stirred at 90 °C for 12 h. The reaction was monitored by TLC, and upon completion, the solvent was evaporated and the residue was purified by flash chromatography on silica gel (Hex:AcOEt).

Compounds **14** and **15**: A mixture of the appropriate heterocyclic 1,3-dinucleophile (5-amino-1*H*-pyrazole-4-carbonitrile or 4*H*-1,2,4-triazole-3,5-diamine; 1.5 eq), the corresponding aldehyde (2-thiophenecarboxaldehyde or 3-thiophenecarboxaldehyde; 1 eq), β-ketoester (ethyl 3-oxobutanoate or isopropyl 3-oxobutanoate; 1 eq), and chloroacetic acid (0.1 eq) in DMF (3 mL) was stirred at 90 °C for 15 h. The reaction was monitored by TLC, and upon completion, the solvent was evaporated and the residue was purified by flash chromatography on silica gel (Hex:AcOEt).

2.2. Chromatography

The analytical HPLC measurements were performed on a Waters 1525 HPLC System equipped with a Waters 2487 variable-wavelength UV-Vis detector and a Waters 717 plus autosampler. The chromatographic data were acquired using the Waters Breeze Software (Waters, Milan, Italy). Chromatographic separations were performed on the teicoplanin-based column Chirobiotic™ TAG (250 × 4.6 mm id, 5 µm particle size) from ASTEC (Whippany, NJ, USA). Analyses were also carried out by using three commercial Pirkle-type CHIREX® columns (50 × 4.6 mm id, 5 µm particle size), namely (*R*)-1-naphtylglycine and 3,5-dinitrobenzoic acid (CSP-1), (*S*)-Valine and (*R*)-1-(α-naphthyl)ethylamine (CSP-2), and (*S*)-tert-Leucine and (*R*)-1-(α-naphthyl)ethylamine (CSP-3), from Phenomenex (Castel Maggiore, Bologna, Italy). Stock solutions were prepared by dissolving the analytes in MeOH (1 mg/mL). The injection volume was 5 µL and all the chromatographic analyses were performed at room temperature in triplicate. The dead time (t_0) was measured as the retention time of methanol-d_4. The column flow rate was 0.7 mL/min, and the chromatograms were recorded by UV detection at wavelengths of 254 nm and 280 nm. The solvents for mobile phases were filtered through a polytetrafluoroethylene (PTFE) or Nylon-66 membrane (0.45 µm) before use. All the DHP analytes (Figure 1) were evaluated with different mobile phases under normal-phase (NP) and polar organic modes (POM).

In the competition experiments, *N*-acetyl-D-alanine (NADA) was added directly in the mobile phase. Three different concentrations of competitor were tested: 0.1–0.5% and 1%.

2.3. X-ray Crystallography

X-ray diffraction data were collected at the I03 Beamline of the Diamond Light Source, UK (wavelength 0.7293 Å, temperature 100 K, detector DECTRIS PILATUS3 S 6M). The XDS program [24] was used to perform data reduction, while POINTLESS and AIMLESS programs [25] were used for space group identification, scaling, and merging of diffraction data.

TAG crystallised in the space group C2, with one molecule in the asymmetric unit (85 non-H atoms); unit cell parameters a = 35.72 Å, b = 13.11 Å, c = 21.71 Å, and β = 123.34. The Matthews coefficient of such crystals (Vm) is 1.76 Å^3/Da and the solvent content is equal to 30%. The structure solution was achieved by the Modern Direct Methods (MDM) ab initio phasing procedure implemented in the package SIR2014 [26]. It was preliminarily refined by the SHELXL full-matrix least-squares technique based on F^2 [27], by using reflections with $I \geq 2\sigma(I)$ (7457/9030). Non-hydrogen atoms were refined with anisotropic thermal parameters. As a final step, DMSO and water molecules were manually added by using the graphics program COOT [28] and iteratively refined by using REFMAC5 [29]. Atomic coordinates and structure factor amplitudes of TAG were deposited in the Protein Data Bank with PDB ID code 6TOV. Data collection and structure refinement parameters are summarised in Table S4 and the crystal structure is shown in Figure S1 (Supplementary Materials).

2.4. Molecular Docking and Molecular Dynamics Calculations

The molecular skeleton of DHP compounds were built within the MAESTRO software package [30] with standard values of bond lengths and valence angles, and then passed to OPENBABEL [31] for 10,000 steps of steepest descent minimisation using the Universal Force Field. Six representative DHP derivatives among those listed in Figure 1 were chosen, considering three resolved (**6**, **8**, and **9**) and three not-resolved (**12**, **13**, and **15**) compounds, each in its two enantiomers. Docking calculations were performed on each of them considering the resolved TAG crystal structure, herein determined as the target. The *molcharge* complement of QUACPAC [32] was used to achieve Marsili–Gasteiger charges for both chiral selector and selectands. The affinity maps were calculated on a 0.375 Å spaced 85 × 85 × 85 Å^3 cubic box centred on the TAG crystal structure, and the accessibility of the binding site was explored throughout 1000 runs of the Lamarckian Genetic Algorithm (LGA) implemented in AUTODOCK 4.2.6 [33] using the GPU-OpenCL

algorithm version [34], the population size and the number of energy evaluation figures were set to 300 and 10,000,000, respectively. All the achieved hits were clustered according to a RMSD threshold <2.0, and afterwards the best energy and most populated group was selected as input for further molecular dynamics (MD) calculations for monitoring the time-dependence of the interactions of the derivatives with the chiral selector using DESMOND [35].

The TAG/DHP complexes were assembled with the system builder tool implemented in Maestro [36] into an orthorhombic box filled with methanol as the explicit solvent. All simulations were performed on a NVDIA Quadro M4000 GPU at a constant temperature (300 K) and pressure (1 bar) for a total of 1 μs using the default settings and relaxation protocol of DESMOND, with energy and time steps for trajectory recording intervals of 0.5 ps, and to mimic the effect of the anchoring stationary phase, a harmonic constraint of 100 kcal/mol was applied on the TA Csp^3 carbon. From the achieved trajectories, a total number of 2000 frames were afterwards sampled for the data set calculations.

MD trajectories have been analysed by Principal Component Analysis (PCA) implemented in the program RootProf [37] and by scripts of the VMD program [38].

3. Results and Discussion

3.1. Chiral Separation with Pirkle-Type Chiral Stationary Phases (CSPs)

Pirkle-type CSPs are designed for achieving enantiomeric separations exploiting π-π stacking interactions between electron-rich and electron-deficient aromatic systems as the primary attractive interaction forces. Besides the aromatic ones, polar and H-bonding interactions, as well as steric repulsive factors, can play a role in modulating the enantioselective recognition of racemic selectands by chiral selectors in Pirkle-type HPLC columns [39].

The structures of the Pirkle-type CSPs, which differ for the π-acceptor/donor group, and α-amino acid linked through a *n*-propyl bridge to the silica matrix, are shown in Figure 3. Preliminarily, for some representative racemic compounds the mobile-phase composition varied from Hex-EtOH (95:5, *v*/*v*) to more polar mixtures, such as MeOH (100%, *v*/*v*) or MeOH/H_2O (95:5, *v*/*v*) mixtures, which resulted in significant decreases of the chromatographic selectivity. Therefore, the mobile phase was fixed as Hex-EtOH (95:5, *v*/*v*) and all the fifteen racemic DHPs were analysed at room temperature and flow rates of 0.7 mL/min. The chromatographic data, k_1 and α values, are summarised in Table 1.

Table 1. Chromatographic data: retention factors of first eluted enantiomer (k_1) and separation factor (α) for the chiral DHP analytes on Pirkle-type CSPs in fixed experimental conditions [a].

Analyte	CSP 1		CSP 2		CSP 3	
	k_1	α	k_1	α	k_1	α
1	5.07	1	2.51	1.15	2.38	1.17
2	23.0	1.09	11.0	1.11	10.4	1.09
3	19.9	1.23	7.70	1	6.67	1.06
4	15.7	1.21	5.61	1	4.86	1.06
5	23.5	1	20.3	1	22.6	1
6	8.22	1.09	5.06	1.22	4.24	1.27
7	11.5	1	11.2	1.05	6.13	1.11
8	6.97	1.08	5.34	1.06	3.85	1.12
9	6.92	1.08	6.17	1.07	4.34	1.09
10	2.00	1	0.93	1.43	1.06	1.43
11	11.0	1.40	4.37	1.24	4.27	1.38
12	2.25	1.22	0.98	1.39	0.99	1.51
13	11.5	1.12	7.08	1.08	6.62	1.13
14	5.82	1.17	2.19	1	1.62	1
15	17.03	1	5.66	1.1	4.59	1.18

[a] Mobile phase: *n*-Hex-EtOH (95:5, *v*/*v*); flow rate: 0.7 mL·min^{-1}; room temperature; UV detection: 254 nm.

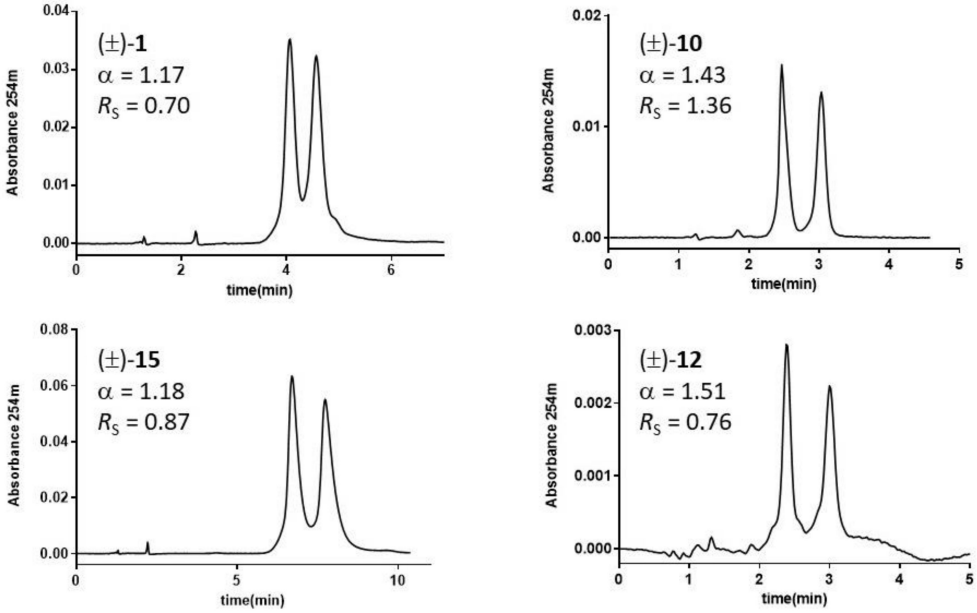

Figure 3. Chromatograms of DHP analytes **1**, **10**, **12**, and **15** on Pirkle-type 3020-(*S*)-*tert*-leucine and (*R*)-1-(α-naphthyl)ethylamine (**CSP-3**) columns. Mobile phase: Hex-EtOH (95:5, *v*/*v*); flow rate: 0.7 mL/min; room temperature; UV detection: 254 nm.

The Pirkle-type CPSs, in the given experimental conditions, separated the majority of the racemic DHPs selectands, but in no case a baseline resolution was obtained. The α values achieved with CSP1, bearing the π-acidic 3,5-dinitro benzoyl (3,5-DNB) moiety and napht-2-yl as amino acid sidechain, did not correlate at all with α values determined on CSP2 (r^2 = 0.006) and CSP3 (r^2 = 0.061), which in turn, given their more similar chemical structures, returned linearly related α values (r^2 = 0.923), with a slope close to unity (1.09) and an intercept close to zero (−0.05). CSP3, bearing napht-2-yl as the only aromatic binding site and *t*-butyl as the amino acid side-chain, provided slightly better enantiomeric separation of the examined DHP chiral derivatives, as (i) only two racemic compounds were not separated (in contrast to four and five non-resolved racemic selectands with CSP2 and CSP1, respectively), and (ii) the spread of the α ratios (Δα = 0.45) was slightly larger compared with CSP2 (Δα = 0.38) and CSP1 (Δα = 0.32).

Due to the methylation of N1, the racemic compound **5** is not separated on any of the three Pirkle-type columns, highlighting the critical role of the H-bond achieved by N1-H as HB donor. Compounds **10**, **11**, and **12**, which are among the bulkiest molecules in the investigated series, achieved better enantioselective separation with CSP2 and CSP3, bearing branched amino acid sidechains like *i*-Pr and *t*-Bu, respectively. HPLC traces on CSP3 for some diverse DHP derivatives, along with enantioselectivity α and resolution R_S values, are shown in Figure 3.

Overall, the chiral HPLC data from the three-Pirkle-type CSPs in NP mode suggest that through replacing the π-acidic 3,5-DNB aromatic binding site in CSP1 and gradually introducing a site of steric repulsive interaction, namely the sidechains *i*-Pr (CSP2) and *t*-Bu (CSP3), the retention times tend to diminish, and separation factors (α) tend to increase. Within the limits of the chemical space explored, CSP3 appears a more suitable and versatile Pirkle-type column for chiral DHP derivatives. However, in no case was a baseline separation achieved, but there should be room for improvement aimed at preparative applications.

3.2. Chiral Separation with Teicoplanin Aglycone Selector

Macrocyclic glycopeptide antibiotics have been successfully used as versatile and selective tools for enantioseparation, evaluation of enantiomeric purity, and the pharmacokinetic studies of a great variety of chiral molecules. Multiple stereogenic centres,

different functional groups, and primarily inclusion cavities are responsible for the good outcomes of these CSPs [40].

In this study the separation of the enantiomeric DHP mixtures was performed with a Chirobiotic^{TM} TAG column under a polar organic mode where MeOH, EtOH, and MeOH-ACN (50:50, *v*/*v*) were used as mobile phases. Different proportions of EtOH-ACN and MeOH-H_2O were preliminarily evaluated for a few racemic DHP-based selectands (Table S1, Supplementary Materials).

The TAG chiral selector consists of four fused rings forming a semi-rigid 'basket' that contains seven aromatic rings, two of which bear chloro-substituents and five bear phenol groups (Figure 2). The HPLC results obtained on TAG-based column eluting with the above mobile phases are summarised in Table 2, whereas the chromatograms of racemic DHP analogs are shown in Figure 4.

Table 2. Chromatographic data: retention factors of the first eluted enantiomer (k_1) and separation factor (α), for the chiral DHP analytes on a Chirobiotic^{TM} TAG column with three organic polar mobile phases [a].

Analyte	A		B		C	
	k_1	α	k_1	α	k_1	α
1	0.72	4.24	2.13	4.00	0.66	2.65
2	0.84	3.88	2.46	2.75	0.64	2.55
3	0.86	2.96	2.40	2.42	0.61	2.90
4	0.89	1.61	2.17	1.58	0.61	1.46
5	0.73	1	1.9	1	0.63	1
6	0.22	2.41	0.50	2.12	0.14	1.64
7	0.32	2.00	0.56	2.28	0.31	1.32
8	0.47	8.76	0.85	9.68	0.26	4.77
9	0.46	6.04	0.94	5.52	0.21	3.67
10	0.27	1	0.37	1	0.24	1
11	0.46	1.50	0.94	1.45	0.18	1.11
12	0.35	1	0.52	1	0.30	1
13	0.79	1	2.32	1	0.66	1
14	0.28	1	0.41	1	0.15	1
15	0.40	1	0.75	1	0.38	1

[a] Mobile phases: A = MeOH, B = EtOH and C = MeOH-ACN (50:50, *v*/*v*); flow rate: 0.7 mL·min^{-1}; room temperature; UV detection: 254 nm.

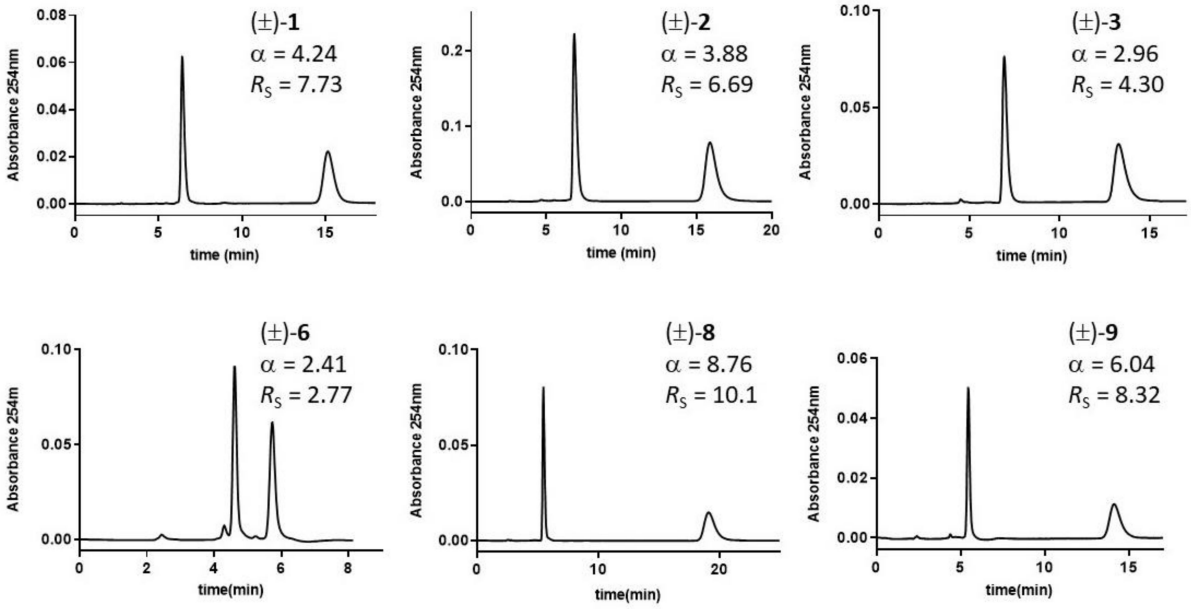

Figure 4. Chromatograms of DHP analytes on Chirobiotic^{TM} TAG column. Mobile phase: MeOH 100%, *v*/*v*; flow rate: 0.7 mL·min^{-1}; room temperature; UV detection: 254 nm.

The majority of racemic DHP mixtures (60%) achieved on TAG-based CSP baseline enantiomer separations showed in some cases (e.g., *rac*-**8** and *rac*-**9**) excellent enantioselectivity ratios ($\alpha > 6$) and *Rs* values from 2 to 10. With *rac*-**6**, the previously resolved (*R*)-enantiomer was the most retained one (Figure S2, Supplementary Materials. The decrease of polarity of the mobile phase from MeOH 100%, *v*/*v*, to EtOH 100%, *v*/*v*, and the mixture MeOH/ACN (50:50, *v*/*v*) does decrease α values. The three-mobile-phase-furnished enantioseparation factors were highly intercorrelated ($r^2 > 0.88$). However, better separations were obtained with MeOH (A) and EtOH (B). The α values, which spanned a range of about 7.8 and 8.7 units with MeOH and EtOH, respectively, was linearly interrelated ($r^2 = 0.966$), with a slope close to unity (1.03), and an intercept equal to -0.17. The low toxicity of the solvents examined, compared to those generally employed in NPM, is an advantage to be considered.

The molecules under investigation are not congeneric; therefore, structure–enantioselectivity relationships (QSERs) are not always clearly explainable. Looking at the α values determined using MeOH as eluent (and EtOH as well), the best enantiomers resolution was achieved with the racemic analytes **8** and **9**, most likely because of the fused 1*H*-tetrazole ring bearing three further H-bond acceptor sites. In contrast, the loss of a critical H-bond donor group, due to the methylation of N1, may explain the lack of enantioselectivity of the TAG chiral selector toward *rac*-**5**. Repulsive steric effects experienced by the selectands into the TAG chiral basket(s) may cause the lack of enantiomeric resolution of DHP derivatives **10**, **12**, **14**, and **15** ($\alpha = 1$) and the poor enantioseparation ($\alpha = 1.50$) of **11**.

To account for steric effects, H-bonding, and polar interactions, the following molecular descriptors were calculated and collected in Table S2 (Supplementary Materials) for the whole set of DHP analytes: MV (molar volume), MSA (molecular surface area), PSA (polar surface area), HBA (count of H-bond acceptors), and HBD (count of H-bond donors). The squared correlation matrix of the enantioseparation factor and calculated descriptors of *rac*-**1**–**15** (Table S3) shows that, excluding the expected correlations of MV with MSA ($r^2 = 0.723$) and PSA with HBA count ($r^2 = 0.858$), no other noteworthy correlation exists among the molecular descriptors and between single descriptors and α value. Nevertheless, there must be a detrimental effect of bulkiness, as assessed by MV and MSA, on the enantioselectivity of TAG. As matter of fact, poorly or non-separated compounds ($\alpha < 1.5$), i.e., **10**, **11**, **12**, **14**, and **15**, have MSA values volumes falling within the area of 473 ± 13 Å^2, whereas better separated 4-substituted DHPs ($\alpha > 2$; **1**–**4** and **6**–**9**) have MSAs equalling 417 ± 38 Å^2. A similar trend can be inferred from the calculation of the mean MV $\pm$ SD. In contrast, no difference in the mean value of PSA, accounting for 'attractive' intermolecular forces, for the two clusters of compounds, which is 87 ± 15 Å^2 and 85 ± 13 Å^2, were found for the two groups of selectands achieving $\alpha < 2$ and $\alpha > 2$, respectively. This trend suggests that DHP derivatives with sizes larger than a threshold value (reasonably, MSA > 460 Å^2) could not access the TAG cleft, where highly directional polar and H-bond interactions may favour enantiomer separations.

Two remarkable exceptions to the above rules are represented by *rac*-**5** (MSA = 443 Å^2) and *rac*-**13** (MSA = 354 Å^2), which, despite their bulkiness under the threshold, did not achieve any enantiomer separation. While the lack of an N1-H HBD group could explain the lack of enantiomer separation with 5, the absence of the enantioselective binding of 13 into the TAG chiral selector cleft was not so obvious. Compound **13**, with its MSA clearly below the threshold value of 460 Å^2, should enter the chiral cleft of TAG. It cannot be excluded that the S atom of the thiophen-3-yl group at the chiral C4, compared with the O atom in the furanyl moiety in other DHPs examined herein, serves as a poorer H-bond acceptor, due to unsuitable bond length and angles [41].

Teicoplanin-related antibiotics exert their activities because they stereospecifically bind to the precursor peptidoglycan peptide terminus *N*-acetyl-D-Ala-D-Ala during bacterial cell wall biosynthesis. *N*-acetyl-D-alanine (NADA) is capable of binding specifically to the pocket of TAG, and therefore was used as a competing agent in displacement studies. The

displacement concept was applied to investigate the enantioselective and non-selective binding of test analytes on the Chirobiotic™ TAG column [42].

Interestingly, the competition experiments performed on *rac*-6 showed the retention factor of the more retained enantiomer (k'_2), and α value decrease when the concentration of NADA added to the mobile phase increases, thus suggesting that the enantiorecognition of the examined analytes takes place mainly through HBs and polar interactions in the same site where the terminal D-Ala of the 'natural' ligand binds. As shown in Figure 5, the experiment translates graphically with the tendency of the chromatographic peaks to coalescence.

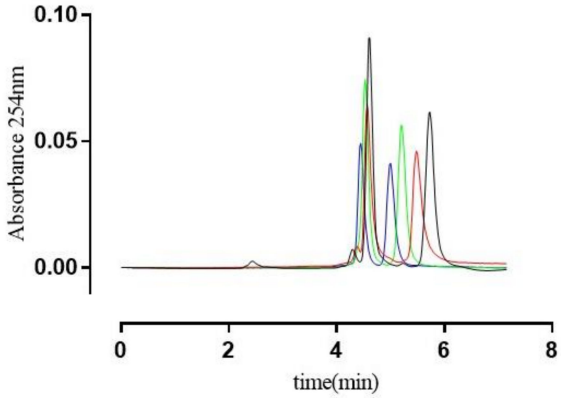

Mobile phase	k'_1	k'_2	α
MeOH	0.22	0.53	2.41
MeOH + NADA 0.1%	0.22	0.47	2.14
MeOH + NADA 0.5%	0.21	0.39	1.86
MeOH + NADA 1.0%	0.21	0.36	1.71

Figure 5. Superposition of chromatograms of (±)-**6** on TAG-based CSP using MeOH 100%, *v*/*v* as the mobile phase containing increasing concentrations of *N*-acetyl-D-Ala (NADA). Retention factors of the first and second eluted enantiomers (k'_1 and k'_2), and separation ratios (α) are summarised in the table; flow rate: 0.7 mL·min^{-1}; room temperature; UV detection: 254 nm.

3.3. Molecular Dockings of Selectands

For better understanding the intermolecular forces mainly responsible for the enantioselective recognition of 4-aryl DHPs by the TAG chiral selector, molecular docking and molecular dynamics calculations were performed with four racemic compounds (i.e., **6**, **8**, **9**, and **12**) chosen, exploring the range of α values (MeOH) from 8.76 (**8**) to 1 (**12**). The high-resolution (0.77 Å) X-ray crystal structure of TAG (Figure 6) was solved, deposited in the Protein Data Bank (PDB ID code: 6TOV) and used in molecular docking calculations with molecular models of the investigated 4-aryl DHP-containing selectands.

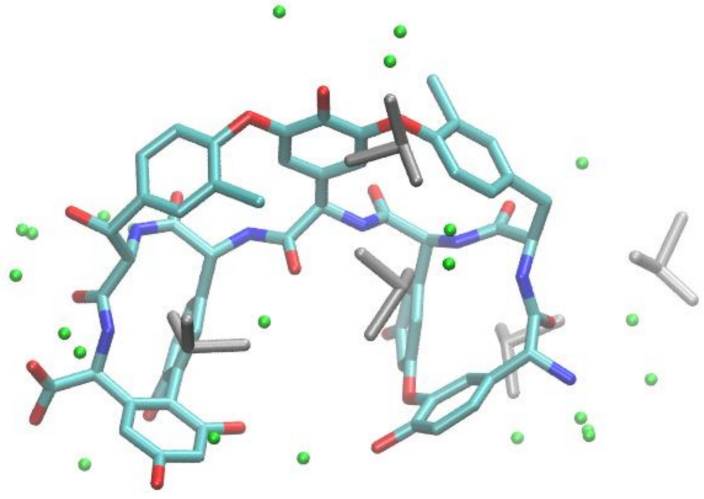

Figure 6. X-ray crystal structure of teicoplanin aglycone (TAG) (oxygen, red; nitrogen, blue; carbon, cyan) with DMSO (grey) and water molecules (green spheres).

The computational study allowed us to check for any kind of shape- and atom-type complementarities between the selectands and their anchoring points on the CS molecular surface, and at the same time to achieve plausible and low energy conformations for TAG–DHP complexes that might further constitute input for MD runs. In more detail, the selectands **6**, **8**, **9**, and **12** were initially docked into the basket-like cavity of TAG, and the relative energies of binding, together with a breakdown for the different contributions arising from the key attractive and/or repulsive interactions, were evaluated (Table 3). Starting from these data, timeline monitoring of geometrical and chemical features of TAG-selectands' interactions were indeed deduced from the analysis of MD trajectories carried out with principal component analysis (PCA).

Table 3. Free energy of binding (FEB) and relative contributions [a] estimated from docking calculations.

cmpd	Chirality	FEB	EFF [a]	VdW + HB + ELE + DES [a]	VdW + HB [a]	ELE [a]	DES [a]
6	*R*	−6.80	−0.296	−7.08	−8.87	0.02	1.78
	S	−7.55	−0.328	−7.60	−9.82	0.04	2.19
8	*R*	−6.74	−0.337	−7.13	−9.03	−0.12	2.02
	S	−6.68	−0.334	−7.07	−8.96	−0.05	1.94
9	*R*	−7.39	−0.352	−7.40	−9.29	−0.05	1.93
	S	−7.36	−0.350	−7.51	−9.43	−0.14	2.06
12	*R*	−7.56	−0.302	−7.38	−9.46	−0.25	2.33
	S	−7.16	−0.286	−7.10	−9.28	−0.26	2.44

[a] EFF, ligand efficiency (FEB/number of heavy atoms); VdW, Van der Walls; HB, hydrogen bond; ELE, electrostatic; DES, desolvation.

As it may be inferred from the docking poses (Figure 7), the binding mode is quite similar for structurally related selectands achieving comparable α values (i.e., **8** and **9**), whereas compounds with a diverse scaffold (i.e., **6** and **12**) substantially fit the TAG surface in a different manner. Indeed, the binding modes of the most retained 4-furanyl DHPs, such as **8** and **9**, are enforced by highly directional H-bonds comprising the nitrogen of the tetrazole ring, with the backbone peptide bond close to the charged N-terminal of TAG; moreover, the furan ring attached to the chiral centre is oriented, depending upon the configuration, towards diverse areas, namely the chlorine atom or the exterior moiety of the TAG basket exposed to solvent. It might be proposed that (*R*)-**8** and (*S*)-**9** should correspond to the most retained enantiomers according to a unique kind of π-π stacking involving the halogen atom and the five-membered heterocyclic rings. In contrast, (*S*)-**8** a®(*R*)-**9** should be more easily eluted by the mobile phase.

Regarding the two other selectands, the above considerations cannot be applied for both the enantiomers in **12**, since it is rather clear from the dockings that it cannot achieve any polar and persistent anchoring interactions due to the steric hindrance (exceeding volume) of the benzimidazole ring, while thiopyrimidinone **6** shows a diverse interaction pattern. The (*R*) configuration obliges the ligand to orient the thiopyrimidinone ring outside the TAG basket, while in the (*S*) configuration it is more deeply embedded in a narrow gorge, and consequently the furan ring stacks with the phenol ring close to the C-terminus of TAG. According to this interpretation, the elution order from the least to the most retained DHP enantiomers (i.e., (*R*)-**12**, (*S*)-**12**, (*R*)-**6**, (*S*)-**6**, (*S*)-**9**, (*R*)-**8**, (*R*)-**9**, and (*S*)-**8**) it is not consistent with the HPLC data. Deeper insights were instead gained from molecular dynamics calculations carried out on the complexes from the docking outputs of both the enantiomers of each virtually investigated DHP selectand. Regardless of the evidence emerging from the PCA hereafter reported, timeline plots of the radius of gyration highlighted some intriguing insights and divergences (Figure S4, Supplementary Materials). Both enantiomers of **8** and **9** are constantly patched on TAG, and this also applies to (*R*)-**6** in the first 200 ns. On the contrary, (*S*)-**6**, (*R*)-**12**, and (*S*)-**12** are substantially steered out from the basket-like TAG cavity. This may, at least in part, explain the differences in the experimentally determined separation factors of 4-aryl DHPs on TAG CSP.

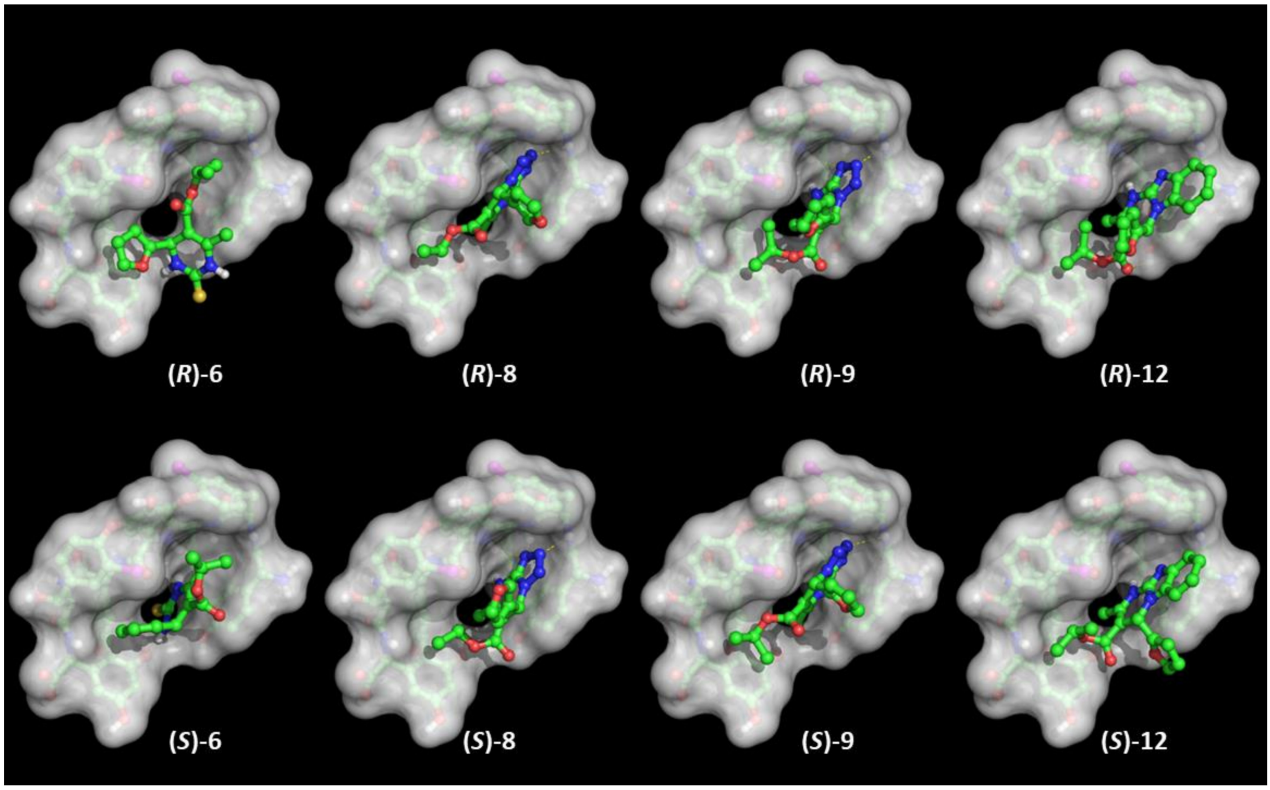

Figure 7. Binding poses of the enantiomers of compounds **6**, **8**, **9**, and **12** to X-ray structure of TAG rendered with transparent solid surface. Molecular models are colored by atom type: C (green), O (red), N (blue), S (yellow); H atoms are not shown.

3.4. Structural Interpretation of the Chiral Separation

The structural determinants of the chiral separation of DHP derivatives by TAG have been further investigated. The persistence of the docking pose, monitored by considering the distance between the barycentre of TAG and DHP selectands, did not appear related to the experimental data (Figure 8). In fact, both enantiomers of **8** and **9** persist on the initial docking position throughout the simulation with an average distance of about 5 Å; both enantiomers of **6**, **12**, and **13** move away from the initial pose, having an average distance of about 15 Å, while the enantiomers of 15 behave differently.

Conformational flexibility, which is instead strongly influenced by the interaction with TAG, was analysed in this study by the following procedure: (i) the molecules are aligned along the trajectory and amended of an initial equilibration time of 200 ns; (ii) the root mean square fluctuation (RMSF) of the DHP atoms is calculated; (iii) RMSF profiles of different compounds are scaled so that they have same average value and standard deviation to account for the different complexities of the compounds (Figure S5 and Table S5 in Supplementary Materials); (iv) scaled fluctuation profiles are compared by PCA. The PCA results are illustrated in Figure 9 (score plots), which shows the distribution of representative points of each compound in the score plots of the first two principal components.

Both enantiomers of compounds **6** and **13** are separated along the first principal component (PC1), explaining about 66% of the total data variance (Figure 9a). These differences are due to the way the molecules move during the simulation, regardless of their relative position with TAG. This could be due to the presence of sulphur (a poorer HBA), or to the specific interactions they have with TAG. To make the set of structures homogeneous, the comparative analysis of RMSF profiles has been repeated without these compounds (Figure 9b). In this case, PC1, which accounts for 61.2% of the total variance, clearly separates the (*R*)-enantiomers of **8** and **9**, while the same does not occur for the enantiomers of **12** and **15**, in full agreement with the experimentally observed

chiral separation. Therefore, the fluctuation of the atomic positions of the common DHP nucleus, as influenced by the presence of TAG, regardless of whether the selectand remains bound to it or not, can explain the observed chiral separation. It is worth noting that the chiral separation of **8** and **9** was already present in Figure 9a but hidden by the presence of heterogeneous compounds **6** and **13**. Individual RMSF profiles, grouped according to clusters shown in Figure 9, are reported in Supplementary Materials (Figure S4).

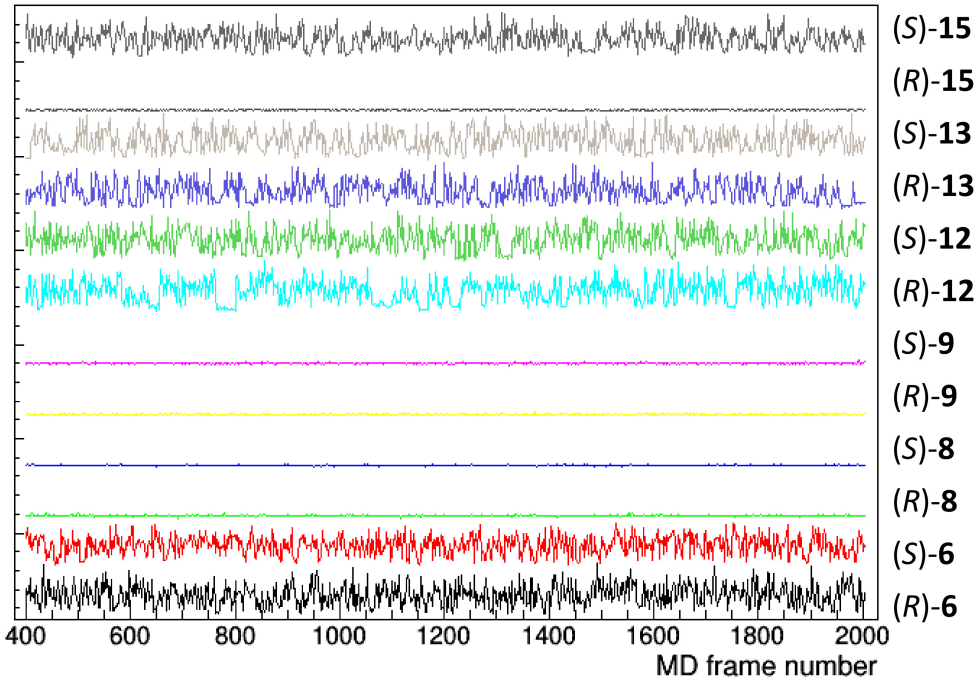

Figure 8. Distance between TAG and the compound barycentre as a function of the frame number of the MD trajectory (1 frame = 0.5 ns). Initial 400 frames, corresponding to 200 ns, have been not considered to account for system equilibration.

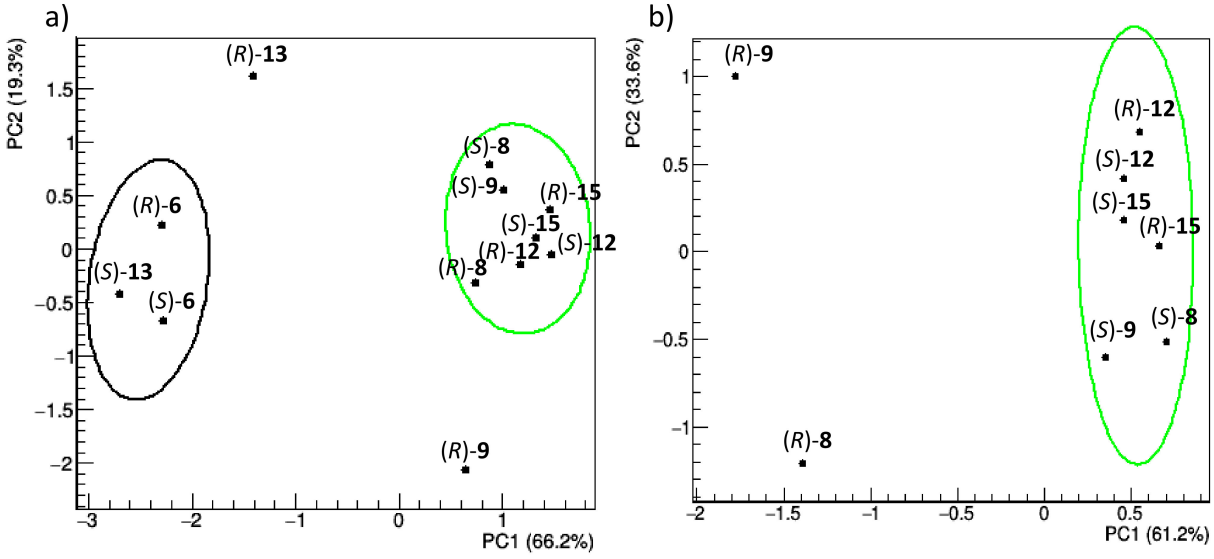

Figure 9. Score plots of the first two principal components obtained by PCA applied to RMSF profiles of the (*R*) and (*S*) enantiomers of racemic **6**, **8**, **9**, **12**, **13**, and **15** (**a**) and **8**, **9**, **12**, and **15** (**b**). Representative points of each enantiomer are grouped according to a hierarchic clustering algorithm; 85% confidence level ellipses are shown. The percentage of the data variance explained by each principal component is reported in parentheses on the axes.

To possibly gain further insight into the molecular features favouring the chiral separation, we compared the solvent accessibility of the two enantiomers in the whole conformer population sampled by MD calculations. The ratio between the solvent-accessible surface areas (SASA) of the DHP atoms of the (*R*) and (*S*) enantiomers is shown in Figure 10, which indicates, albeit not a statistically significant trend, the largest deviation from unity for compounds **8** and **9**.

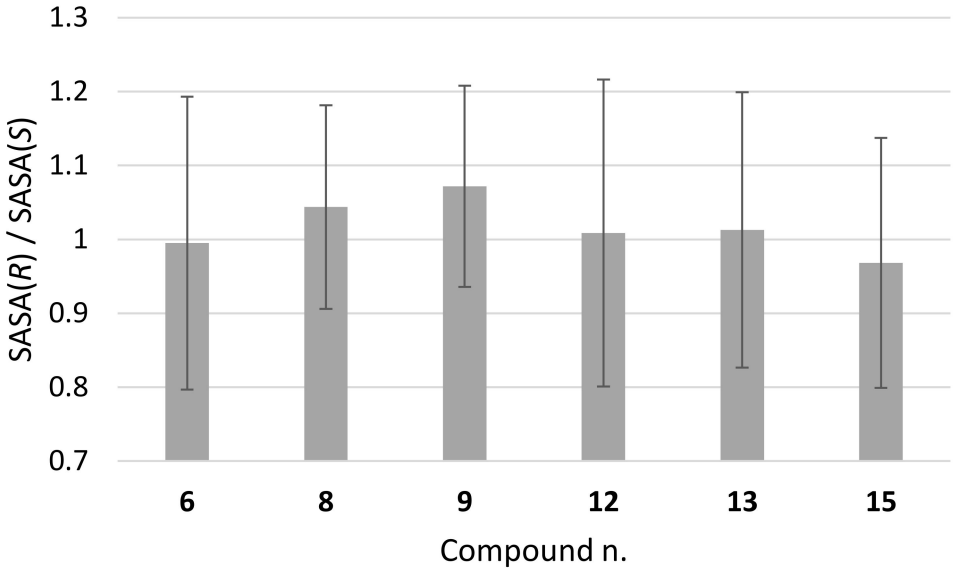

Figure 10. Ratio between average values of solvent accessible surface area (SASA) of (*R*) and (*S*) enantiomers, as calculated from MD simulations.

4. Conclusions

Chirobiotic^{TM} TAG, a CSP bearing teicoplanin aglycone as the chiral selector, and 100%, *v*/*v* MeOH or EtOH as the mobile phase in PO conditions, proved to be a suitable method for the efficient enantiomer resolution of several 4-aryl-3,4-dihydropyrimidin-2(1*H*)-one (DHP) alkoxycarbonyl esters, pharmacologically active as A_{2B} adenosine receptor antagonists. Compared to three herein examined Pirkle-type CSPs, eluted in normal mode, the TAG-based CSP provided a baseline separation and high enantioselectivity factors ($\alpha > 2$) for the majority (60%) of the fifteen diverse racemic DHP derivatives investigated, demonstrating in those cases high potential for preparative purposes.

Quantitative information analysis of calculated molecular descriptors of size and polar/H-bonding interactions shed light on the main repulsive (steric effects) and attractive (H-bonds—polar and apolar) intermolecular interactions governing the binding of DHP selectands and the TAG chiral selector. Within the limits of the explored physicochemical space, it appears that only compounds with MV < 260 Å^3 and MSA < 460 Å^2 may enter the chiral cleft/cavities of TAG and form enantioselective H-bonds, both polar and apolar (e.g., π-stacking) interactions, which stabilize the selectand/selector complexes. Bulkier compounds (MV > 280 Å^3, MSA > 470 Å^2) should be less likely to form complexes with TAG that are stable over time. PSA or a count of H-bonding atoms, taken individually, are unable to distinguish between separated and non-separated DHP selectands.

Useful insights into the mechanism of chiral separation on TAG-based CSP were obtained by molecular dynamics calculations on selector-selectand, as obtained by docking calculation. Multivariate analysis (PCA and clustering) of MD simulation data revealed that the movements of the DHP selectands in the simulation box are influenced by the presence of TAG, even if they are not closely bound to it. Structural determinants, such as positional fluctuation and solvent accessibility to 4-aryl DHP selectands, were found to be related to the observed chiral separation.

Supplementary Materials: The following supporting information can be downloaded at https://www.mdpi.com/article/10.3390/separations9010007/s1, Figures S1–S5 and Tables S1–S5 showing graphics/plots or collecting data related to HPLC chiral separation, X-ray crystal structure of teicoplanin aglycone, molecular descriptors, molecular dynamics trajectories, etc.

Author Contributions: Conceptualisation, I.B., A.C., R.C., S.C. and C.D.A.; methodology, I.B., A.C., B.C., B.D.B., R.C. and S.C.; software, A.C., R.C. and C.D.A.; investigation, I.B., R.P., A.C., B.C., B.D.B., R.C. and S.C.; data curation, I.B., R.P., M.C., M.M., E.S., S.C. and C.D.A.; writing—original draft preparation, I.B., M.M., A.C., R.C. and S.C.; writing—review and editing, M.C., R.C., S.C. and C.D.A.; supervision, S.C. and C.D.A.; funding acquisition, R.P., A.C., M.C. and C.D.A. All authors have read and agreed to the published version of the manuscript.

Funding: This research was financially supported by the Italian Ministry of Universities and Research (Progetti di Rilevante Interesse Nazionale-Call 2017, PRIN 2017, Grant 201744BN5T_004).

Institutional Review Board Statement: Not applicable.

Informed Consent Statement: Not applicable.

Data Availability Statement: Not applicable.

Acknowledgments: The authors gratefully acknowledge the instrumental support of the University of Bari Aldo Moro, Department of Pharmacy–Pharmaceutical Sciences, and the Institute of Crystallography, Italian National Council of Research (C.N.R.), Bari. The authors gratefully acknowledge the Diamond Light Source for the provision of beamtime (proposal number MX15832).

Conflicts of Interest: The authors declare no conflict of interest.

Abbreviations

DHP, 3,4-dihydropyrimidin-2(1*H*)-one; CSP, chiral stationary phase; NARP, non-aqueous reversed phase; NP, normal phase; NADA, *N*-acetyl-d-alanine; TAG, teicoplanin aglycone; TE, teicoplanin; MeOH, methanol; EtOH, ethanol; IPA, isopropanol; ACN, acetonitrile; Hex, hexane.

References

1. Calcaterra, A.; D'Acquarica, I. The market of chiral drugs: Chiral switches versus de novo enantiomerically pure compounds. *J. Pharm. Biomed. Anal.* **2018**, *14*, 7323–7340. [CrossRef]
2. Kappe, C.O. Biologically active dihydropyrimidones of the Biginelli-type: A literature survey. *Eur. J. Med. Chem.* **2000**, *35*, 1043–1052. [CrossRef]
3. Kappe, C.O. Recent Advances in the Biginelli dihydropyrimidine synthesis. New tricks from an old dog. *Acc. Chem. Res.* **2000**, *33*, 879–888. [CrossRef] [PubMed]
4. Zhu, J.; Bienayme, H. Asymmetric isocyanide-based MCRs. In *Multicomponent Reactions*, 1st ed.; Wiley-VCH: Weinheim, Germany, 2005.
5. Crespo, A.; El Maatougui, A.; Biagini, P.; Azuaje, J.; Coelho, A.; Brea, J.; Loza, M.I.; Cadavid, M.I.; García-Mera, X.; Gutieŕrez-de-Terań, H.; et al. Discovery of 3,4-dihydropyrimidin-2(1*H*)-ones as a novel class of potent and selective A2B adenosine receptor antagonists. *ACS Med. Chem. Lett.* **2013**, *4*, 1031–1036. [CrossRef] [PubMed]
6. Carbajales, C.; Azuaje, J.; Oliveira, A.; Loza, M.I.; Brea, J.; Cadavid, M.I.; Masaguer, C.F.; García-Mera, X.; Gutiérrez de Terán, H.; Sotelo, E. Enantiospecific recognition at the A2B adenosine receptor by alkyl 2-cyanoimino-4-substituted-6-methyl-1,2,3,4-tetrahydropyrimidine-5-carboxylates. *J. Med. Chem.* **2017**, *60*, 3372–3382. [CrossRef]
7. Crespo, A.; El Maatougui, A.; Azuaje, J.; Escalante, L.; Majellaro, M.; Loza, M.I.; Brea, J.; Cadavid, M.I.; Gutiérrez de Terán, H.; Sotelo, E. Exploring the influence of the substituent at position 4 in a series of 3,4-dihydropyrimidin-2(1*H*)-one A2B adenosine receptor antagonists. *Chem. Heterocycl. Compd.* **2017**, *53*, 316–322. [CrossRef]
8. Mallo-Abreu, A.; Majellaro, M.; Jespers, W.; Azuaje, J.; Caamaño, O.; García-Mera, X.; Brea, J.M.; Loza, M.I.; Gutiérrez-De-Terán, H.; Sotelo, E. Trifluorinated pyrimidine-based A2B antagonists: Optimization and evidence of stereospecific recognition. *J. Med. Chem.* **2019**, *62*, 9315–9330. [CrossRef] [PubMed]
9. El Maatougui, A.; Azuaje, J.; González-Gómez, M.; Miguez, G.; Crespo, A.; Carbajales, C.; Escalante, L.; García-Mera, X.; Gutiérrez de Terán, H.; Sotelo, E. Discovery of potent and highly selective A2B adenosine receptor antagonist chemotypes. *J. Med. Chem.* **2016**, *59*, 1967–1983. [CrossRef]
10. Mallo-Abreu, A.; Prieto-Díaz, R.; Jespers, W.; Azuaje, J.; Majellaro, M.; Velando, C.; García-Mera, X.; Caamaño, O.; Brea, J.; Loza, M.I.; et al. Nitrogen-Walk Approach to Explore Bioisosteric Replacements in a Series of Potent A2B Adenosine Receptor Antagonists. *J. Med. Chem.* **2020**, *63*, 7721–7739. [CrossRef]

11. Majellaro, M.; Jespers, W.; Crespo, A.; Núñez, M.J.; Novio, S.; Azuaje, J.; Prieto-Díaz, R.; Gioé, C.; Alispahic, B.; Brea, J.; et al. 3,4-Dihydropyrimidin-2(1*H*)-ones as Antagonists of the Human A2B Adenosine Receptor: Optimization, Structure–Activity Relationship Studies, and Enantiospecific Recognition. *J. Med. Chem.* **2021**, *64*, 458–480. [CrossRef]
12. Kappe, C.O.; Stadler, A. The Biginelli dihydropyrimidinone synthesis. *Org. React.* **2004**, *63*, 1–116. [CrossRef]
13. Bhosale, R.S.; Wang, T.; Zubaidha, P.K. An efficient, high yield protocol for the one-pot synthesis of dihydropyrimidin-2(1*H*)-ones catalyzed by iodine. *Tetrahedron Lett.* **2004**, *45*, 9111–9113. [CrossRef]
14. Reddy, K.R.; Reddy, C.V.; Mahesh, M.; Raju, P.V.K.; Narayana Reddy, V.V. New environmentally friendly solvent free synthesis of dihydropyrimidinones catalysed by *N*-butyl-*N*,*N*-dimethyl-α-phenylethylammonium bromide. *Tetrahedron Lett.* **2003**, *44*, 8173–8175. [CrossRef]
15. Balalaie, S.; Soleiman-Beigia, M.; Romingerb, F. Novel one-pot synthesis of new derivatives of dihydropyrimidinones and unusual polysubstituted imidazolin-2-ones: X-ray crystallographic structure. *J. Iran. Chem. Soc.* **2005**, *2*, 319–329. [CrossRef]
16. Berthod, A.; Chen, X.; Kullman, J.P.; Armstrong, D.W.; Gasparrini, F.; D'Acquarica, I.; Villani, C.; Carotti, A. Role of the Carbohydrate Moieties in Chiral Recognition on Teicoplanin-Based LC Stationary Phases. *Anal. Chem.* **2000**, *72*, 1767–1780. [CrossRef] [PubMed]
17. Jandera, P. Comparison of various modes and phase systems for analytical HPLC. In *Separations Methods in Drug Synthesis and Purification*; Valkò, K., Ed.; Elsevier: Amsterdam, The Netherlands, 2000; pp. 1–71.
18. Péter, A.; Arki, A.; Tourwé, D.; Forró, E.; Fülöp, F.; Armstrong, D.W. Comparison of the separation efficiencies of chirobiotic T and TAG columns in the separation of unusual amino acids. *J. Chromatogr. A* **2004**, *1031*, 159–170. [CrossRef] [PubMed]
19. Berthod, A.; Xiao, T.L.; Liu, Y.; McCulla, R.D.; Jenks, W.S.; Armstrong, D.W. Separation of chiral sulfoxides by liquid chromatography using macrocyclic glycopeptide chiral stationary phases. *J. Chromatogr. A* **2002**, *955*, 53–69. [CrossRef]
20. Altomare, C.; Carotti, A.; Cellamare, S.; Fanelli, F.; Gasparrini, F.; Villani, C.; Carrupt, P.; Testa, B. Enantiomeric resolution of sulfoxides on a DACH-CNB chiral stationary phase: A quantitative structure-enantioselective retention relationship (QSERR) study. *Chirality* **1993**, *5*, 527–537. [CrossRef]
21. Meričko, D.; Lehotay, J.; Armstrong, D.W. Effect of temperature on retention and enantiomeric separation of chiral sulfoxides using teicoplanin aglycone chiral stationary phase. *J. Liq. Chromatogr. Relat. Technol.* **2006**, *29*, 623–638. [CrossRef]
22. Ravichandrana, S.; Collins, J.R.; Singh, N.; Wainer, I.W. A molecular model of the enantioselective liquid chromatographic separation of (R,S)-ifosfamide and its N-dechloroethylated metabolites on a teicoplanin aglycon chiral stationary phase. *J. Chromatogr. A* **2012**, *1269*, 218–225. [CrossRef]
23. Pisani, L.; Rullo, M.; Catto, M.; de Candia, M.; Carrieri, A.; Cellamare, S.; Altomare, C. Structure-property relationship study of the HPLC enantioselective retention of neuroprotective 7-[(1-alkylpiperidin-3-yl) methoxy]coumarin derivatives on an amylose-based chiral stationary phase. *J. Sep. Sci.* **2018**, *41*, 1376–1384. [CrossRef]
24. Kabsch, W. XDS. *Acta Cryst.* **2010**, *D66*, 125–132. [CrossRef]
25. Winn, M.D.; Ballard, C.C.; Cowtan, K.D.; Dodson, E.J.; Emsley, P.; Evans, P.R.; Keegan, R.M.; Krissinel, E.B.; Leslie, A.G.; McCoy, A.; et al. Overview of the CCP4 suite and current developments. *Acta Cryst.* **2011**, *D67*, 235–242.
26. Burla, M.C.; Caliandro, R.; Carrozzini, B.; Cascarano, G.L.; Cuocci, C.; Giacovazzo, C.; Mallamo, M.; Mazzone, A.; Polidori, G. Crystal structure determination and refinement via SIR2014. *J. Appl. Cryst.* **2015**, *48*, 306–309. [CrossRef]
27. Sheldrick, G.M. Crystal structure refinement with SHELXL. *Acta Crystallogr.* **2015**, *C71*, 3–8.
28. Emsley, P.; Cowtan, K. Coot: Model-building tools for molecular graphics. *Acta Cryst.* **2004**, *D60*, 2126–2132. [CrossRef]
29. Murshudov, G.N.; Vagin, A.A.; Dodson, E.J. Refinement of macromolecular structures by the maximum-likelihood method. *Acta Cryst.* **1997**, *D53*, 240–255. [CrossRef] [PubMed]
30. *Schrödinger Release 2020-4, Maestro*, Schrödinger, LLC: New York, NY, USA, 2020.
31. O'Boyle, N.M.; Banck, M.; James, C.A.; Morley, C.; Vandermeersch, T.; Hutchison, G.R. Open Babel: An open chemical toolbox. *J. Cheminf.* **2021**, *3*, 33. [CrossRef] [PubMed]
32. *QUACPAC 2.1.0.4*, OpenEye Scientific Software: Santa Fe, MX, USA. Available online: http://www.eyesopen.com (accessed on 21 December 2021).
33. Morris, G.M.; Goodsell, D.S.; Halliday, R.S.; Huey, R.; Hart, W.E.; Belew, R.K.; Olson, A.J. Automated docking using a Lamarckian genetic algorithm and an empirical binding free energy function. *J. Comput. Chem.* **1998**, *19*, 1639–1662. [CrossRef]
34. Santos-Martins, D.; Solis-Vasquez, L.; Tillack, A.F.; Sanner, M.F.; Koch, A.; Forli, S. Accelerating AutoDock4 with GPUs and Gradient-Based Local Search. *J. Chem. Theory Comput.* **2021**, *17*, 1060–1073. [CrossRef] [PubMed]
35. Bowers, K.J.; Chow, E.; Xu, H.; Dror, R.O.; Eastwood, M.P.; Gregersen, B.A.; Klepeis, J.L.; Kolossvary, I.; Moraes, M.A.; Sacerdoti, F.D.; et al. Scalable Algorithms for Molecular Dynamics Simulations on Commodity Clusters. In Proceedings of the ACM/IEEE Conference on Supercomputing (SC06), Tampa, FL, USA, 11–17 November 2006.
36. *Maestro-Desmond Interoperability Tools*, Schrödinger: New York, NY, USA, 2020.
37. Caliandro, R.; Belviso, B.D. RootProf: Software for multivariate analysis of unidimensional profiles. *J. Appl. Cryst.* **2014**, *47*, 1087–1096. [CrossRef]
38. Humphrey, W.; Dalke, A.; Schulte, K. VMD: Visual molecular dynamics. *J. Mol. Graph.* **1996**, *14*, 33–38. [CrossRef]
39. Forjan, D.M.; Gazic, I.; Vinkovic, V. Role of the weak interactions in enantiorecognition of racemic dihydropyrimidinones by novel Brush-type chiral stationary phases. *Chirality* **2000**, *19*, 446–452. [CrossRef] [PubMed]

40. Fernandes, C.; Tiritan, M.E.; Cass, Q.; Kairys, V.; Fernandes, M.X.; Pinto, M. Enantioseparation and chiral recognition mechanism of new chiral derivatives of xanthones on macrocyclic antibiotic stationary phases. *J. Chromatogr. A* **2012**, *1241*, 60–68. [CrossRef] [PubMed]
41. Zhou, P.; Tian, F.; Lv, F.; Shang, Z. Geometric characteristics of hydrogen bonds involving sulfur atoms in proteins. *Proteins* **2009**, *76*, 151–163. [CrossRef] [PubMed]
42. Slama, I.; Ravelet, C.; Villet, A.; Ravel, A.; Grosset, C.; Peyrin, E. Displacement study on a vancomycin-based stationary phase using N-acetyl-D-Alanine as a Competing Agent. *J. Chromatogr. Sci.* **2002**, *40*, 83–86. [CrossRef] [PubMed]